Mineralogical Magazine (2023), **87**, 591–598
doi:10.1180/mgm.2023.41

CAMBRIDGE UNIVERSITY PRESS

Article

Tennantite-(Ni), $Cu_6(Cu_4Ni_2)As_4S_{13}$, from Luobusa ophiolite, Tibet, China: a new Ni member of the tetrahedrite group

Yanjuan Wang[1,4], Rujun Chen[2], Xiangping Gu[2*], Zengqian Hou[1,3], Fabrizio Nestola[4], Zhusen Yang[5], Guang Fan[6], Guochen Dong[1], Lijuan Ye[7] and Kai Qu[7,8]

[1]School of Earth Sciences and Resources, China University of Geosciences (Beijing), Beijing 100083, China; [2]School of Geosciences and Info-Physics, Central South University, Changsha 410083, Hunan, China; [3]Institute of Geology, Chinese Academy of Geological Sciences, Beijing 100037, China; [4]Department of Geosciences, University of Padova, Padova 35131, Italy; [5]Institute of Mineral Resources, Chinese Academy of Geological Sciences, Beijing 100037, China; [6]Beijing Research Institute of Uranium Geology, Beijing 100029, China; [7]Tianjin Center, China Geological Survey, Tianjin 300170, China; and [8]School of Earth Sciences and Engineering, Nanjing University, Nanjing 210023, China

Abstract

The new mineral tennantite-(Ni), $Cu_6(Cu_4Ni_2)As_4S_{13}$, has been discovered from the Luobusa Chromitite, Tibet, southwestern China. Tennantite-(Ni) occurs as anhedral grains ranging from 2 to 20 μm in size. In reflected light microscopy, tennantite-(Ni) is isotropic and appears yellow-greenish grey. Reflectance data for Commission on Ore Mineralogy wavelengths in air for tennantite-(Ni) are: 31.0 (470 nm), 29.6 (546 nm), 29.6 (589 nm) and 29.3 (650 nm). Electron microprobe analysis for holotype material gave the empirical formula (on basis of total cations = 16 apfu): $^{M(2)}Cu_6\ ^{M(1)}[Cu_{4.00}(Ni_{0.97}Cu_{0.53}Fe_{0.50})_{\Sigma 2.00}]_{\Sigma 6.00}\ ^{X(3)}(As_{2.94}Sb_{1.06})_{\Sigma 4}S_{12.77}$. Tennantite-(Ni) is cubic, with space group $I\bar{4}3m$ (#217), a =10.2957(9) Å, V = 1091.4(3) Å^3 and Z = 2. By using single-crystal X-ray diffraction, the crystal structure has been determined and refined to a final R_1 = 0.0423 on the basis of 163 independent reflections [$F_o > 4\sigma\ (F_o)$]. The calculated seven strongest powder X-ray diffraction lines [d in Å (I) (hkl)] are: 2.972 (100) (222), 1.820 (83) (440), 2.574 (28) (400), 1.552 (18) (622), 3.640 (10) (220), 1.880 (10) (521) and 1.287 (7) (800). Tennantite-(Ni) is isostructural with other tetrahedrite-group minerals, and nickel is hosted at the tetrahedrally coordinated M(1) site, along with Cu and minor Fe. The mineral and its name have been approved by the Commission on New Minerals, Nomenclature and Classification of the International Mineralogical Association (IMA2021-018).

Keywords: tennantite-(Ni), new mineral, tetrahedrite group, sulfosalt, crystal structure, Luobusa chromitite deposit

(Received 9 November 2022; accepted 22 May 2023; Accepted Manuscript published online: 31 May 2023; Associate Editor: Koichi Momma)

Introduction

Tennantite-series minerals are common and widespread in many ore deposits (Sack *et al.*, 1993; Moëlo *et al.*, 2008). The first discovery of tennantite [tennantite-(Fe)], consisting of the elements Cu, Fe, As and S, was described by the two brothers W. Phillips (1819) and R. Phillips (1819) from England. The tennantite structure was first studied by Pauling and Neuman (1934), who described it in terms of a sphalerite-like configuration. Further studies have shown the tetrahedrite structure (isostructural with tennantite) serves as a framework analogous of sodalite (Belov and Pobedimskaya, 1969; Nyman and Hyde, 1981). Johnson *et al.* (1988) defined the general chemical formula of tetrahedrite as $^{III}M(2)_6\ ^{IV}M(1)_6\ ^{III}X(3)_4\ ^{IV}S(1)_{12}\ ^{VI}S(2)$ (Z = 2), and described the structure as a framework of corner-sharing [$M(1)S(1)_4$] tetrahedra with cages including S(2)-centred $M(2)_6$-octahedra, encircled by four trigonal pyramids [$X(3)S(1)_3$]. Following the current International Mineralogical Association (IMA) nomenclature and classification of the tetrahedrite group, the general chemical formula can be written as $^{M(2)}A_6\ ^{M(1)}(B_4C_2)^{X(3)}D_4\ ^{S(1)}Y_{12}\ ^{S(2)}Z$ (Biagioni *et al.*, 2020); the group is divided into different series on the basis of the A, B, D and Y constituents. The tennantite series is characterised by A and B = Cu^+, D = As^{3+}, Y and Z = S^{2-}. The divalent C constituent at the M(1) site plays the role of a valency-imposed double site-occupancy with the monovalent B constituent in keeping the formula charge balance. Tennantite-(Ni) is the first Ni-dominant species in the tennantite series, other members of this series include tennantite-(Fe) (W. Phillips, 1819; R. Phillips, 1819), tennantite-(Zn) (Des Cloizeaux, 1855; Wuensch *et al.*, 1966), tennantite-(Hg) (Biagioni *et al.*, 2021), tennantite-(Cu) (Biagioni *et al.*, 2022a) and tennantite-(Cd) (Biagioni *et al.*, 2022b). The new species was found in the Luobusa chromite deposit, Qusum County, Tibet, China. The new mineral and its name (symbol Tnt-Ni) have been approved by the Commission on New Minerals, Nomenclature and Classification (CNMNC) of the International Mineralogical Association (IMA2021-018, Wang *et al.*, 2021). The type material is deposited at the Geological Museum of China, No. 16, Yangrou Hutong, Xisi, Beijing 100031, People's Republic of China, under catalogue number M16117.

Corresponding author: Xiangping Gu; Email: guxp2004@163.com
Cite this article: Wang Y., Chen R., Gu X., Hou Z., Nestola F., Yang Z., Fan G., Dong G., Ye L. and Qu K. (2023) Tennantite-(Ni), $Cu_6(Cu_4Ni_2)As_4S_{13}$, from Luobusa ophiolite, Tibet, China: a new Ni member of the tetrahedrite group. *Mineralogical Magazine* **87**, 591–598. https://doi.org/10.1180/mgm.2023.41

Occurrence and mineral description

Tennantite-(Ni) was discovered in the southern Kangjinla district, ~16 km northeast of Qusum County, Tibet, China, in the Luobusa–Kangjinla ophiolite-hosted chromite deposit (29°10′58.0"N, 92°17′47.6"E). The Luobusa–Kangjinla ophiolites include a mantle sequence, a transition zone, and a serpentinite mélange zone (Zhou *et al.*, 1996). The mantle peridotite is mostly composed of harzburgite, with small amounts of dunite and lherzolite. Along the northern boundary fault is a 100–200 m thick transition-zone dunite (Xiong *et al.*, 2015; Yang *et al.*, 2004). The southern portion of the ophiolite contains discontinuous listwanites that are 2–3 km long and 5–30 m wide. From the fault zone to the peridotite, listwanites can be divided into silica-rich listwanites, talc-rich listwanites, and the serpentine zone (Zhang *et al.*, 2015). Tennantite-(Ni) was found in silica-rich listwanites. With the exception of the remaining fragmented magnesiochromite, nearly all of the original minerals in the hand specimen containing the type material have gone, resulting in a light blue to greyish green colour. The most common secondary minerals are dolomite, magnesite, Cr-bearing clinochlore and quartz as the matrix, with a small amount of dispersed annabergite–hörnesite series minerals, antigorite–népouite series minerals and chalcogenides (i.e. gersdorffite, vaesite, chalcostibite, millerite, nickeline, tennantite-(Ni), tetrahedrite-(Ni) and 'tennantite-(Co)' (not yet approved) (Fig. 1a,b).

Tennantite-(Ni) usually occurs as small composite inclusions composed of tennantite-(Ni) and vaesite in gersdorffite. Typically, the anhedral–subhedral granular crystals range in size from 2 to 15 μm (Fig. 1c–f). Tennantite-(Ni) is black in colour

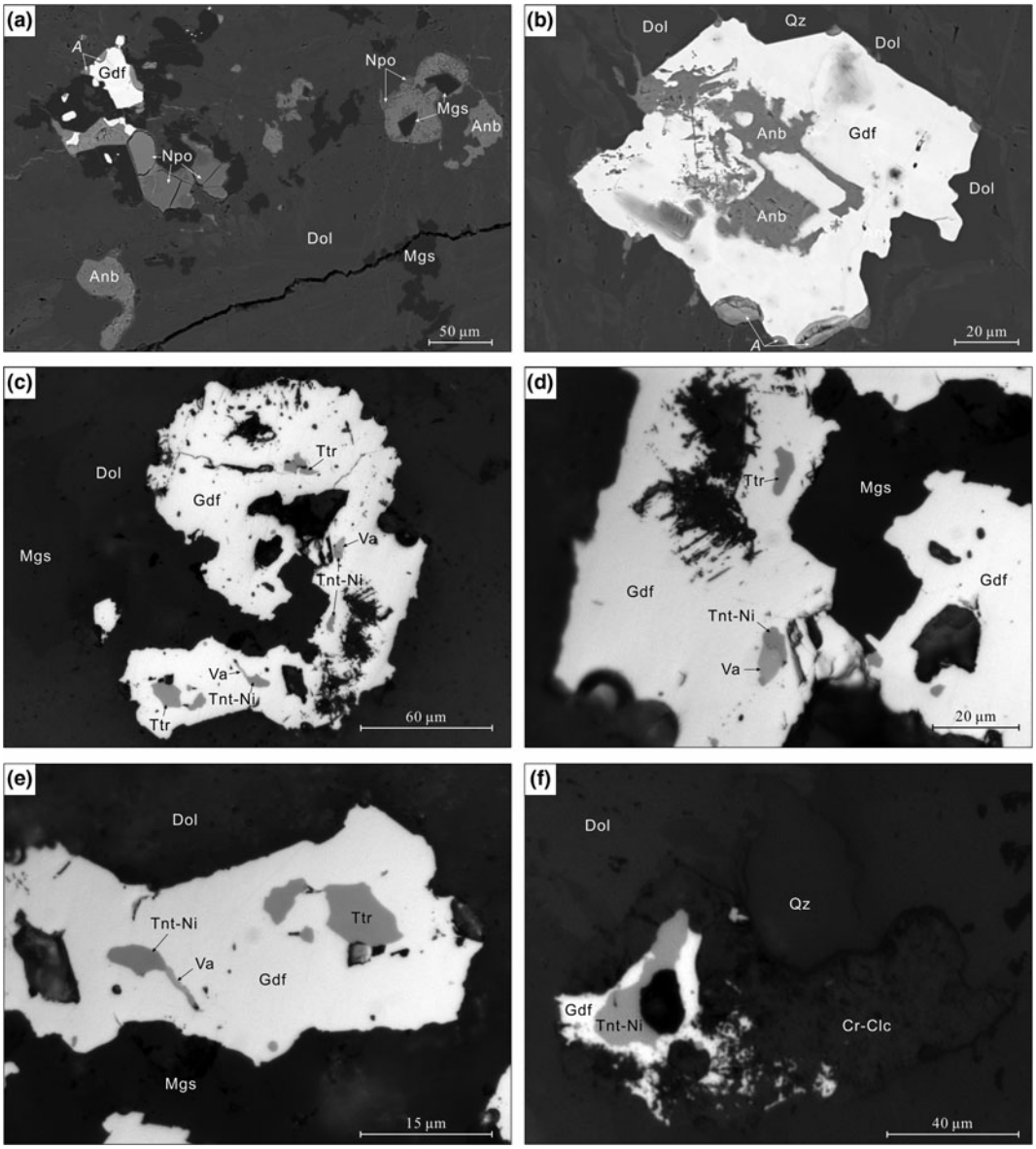

Figure 1. Back-scattered electron (a–b) and plane-polarised reflected light images (c–f, holotype M16117) of the occurrence and mineral association of tennantite-(Ni). Mineral Symbols after Warr (2021). (a) Residual gersdorffite (Gdf) and népouite (Npo) with the secondary annabergite (Anb) and 'nickelkoritnigite' phase (*A*) in magnesite (Mgs), dolomite (Dol) and quartz (Qz) matrix. (b) 'Nickelkoritnigite' phase formed along the edges of the primary gersdorffite, inner partially metasomatic alteration of gersdorffite by annabergite. (c–e) Tennantite-(Ni) (Tnt-Ni), vaesite (Va), tetrahedrite-(Ni) and/or Ni-rich tetrahedrite-(Fe) (Ttr) inclusions within gersdorffite. (f) Gersdorffite was almost completely replaced by Cr-rich clinochlore (Cr-Clc).

https://doi.org/10.1180/mgm.2023.41 Published online by Cambridge University Press

Table 1. Reflectance data for tennantite-(Ni) from the Luobusa chromite deposit.*

λ (nm)	*R* (%)	λ (nm)	*R* (%)
400	36.0	560	29.6
420	34.1	580	29.6
440	32.6	**589 (COM)**	**29.6**
460	31.4	600	29.6
470 (COM)	**31.0**	620	29.6
480	30.6	640	29.4
500	30.1	**650 (COM)**	**29.3**
520	29.8	660	29.1
540	29.6	680	28.6
546 (COM)	**29.6**	700	27.8

*The reference wavelengths required by the Commission on Ore Mineralogy (COM) are given in bold.

with a reddish black streak and the lustre is metallic. Due to the small size of the grain under study, Mohs hardness was not determined, although it is estimated to be 3–3½, in agreement with the hardness of other tetrahedrite-group members. It is brittle, with an indistinct cleavage and a conchoidal fracture. A density of 4.626 g/cm^3 was calculated based on the empirical formula and single-crystal unit-cell parameters. Tennantite-(Ni) is opaque in transmitted light and shows a steel grey colour in reflected light. Internal reflections were not observed. Reflectance values were measured in air using a SiC standard and a Leica microscope with a 20× objective. The four Commission on Ore Mineralogy (COM) wavelengths (*R*) for tennantite-(Ni) are: 31.0 (470 nm), 29.6 (546 nm), 29.6 (589 nm) and 29.3 (650 nm). The complete range of reflectance values is provided in Table 1, and the reflectivity curve for tennantite-(Ni) compared with published data for other tennantite series is shown in Fig. 2.

Raman spectroscopy

The Raman spectrum of tennantite-(Ni) was recorded by using a Renishaw inVia micro-Raman system with a laser with a wavelength of 532 nm, (laser power = 4 mW and beam diameter = 1 μm) in the spectral range from 150 to 1500 cm^{-1} at the Raman Laboratory of Tianjin Center, China Geological Survey. The Raman spectrum was collected *in situ* on the crystal used for the single-crystal X-ray diffraction study from the polished thin section with a 50× objective. The band energies are assigned on the basis of the sequence $\nu_1 > \nu_3 > \nu_2 > \nu_4$, following the guideline by Nakamoto (1997).

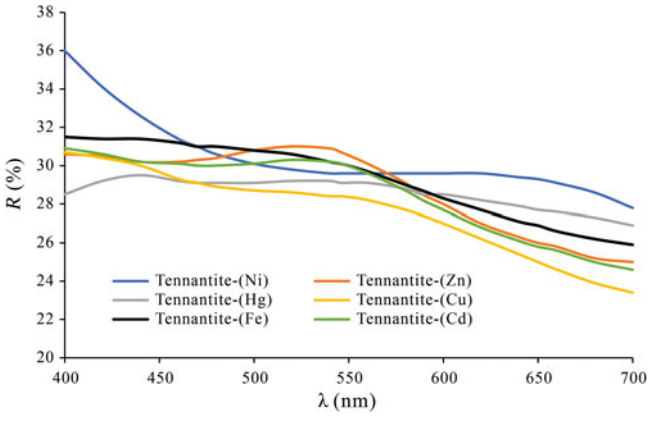

Figure 2. Reflectance curves for tennantite-(Ni) in air. For comparison, the reflectance curves of other members of the tetrahedrite series are shown: tennantite-(Zn) from Tsumeb, Namibia (Criddle and Stanley, 1993); tennantite-(Fe) from Cornwall, U.K. (Criddle and Stanley, 1993); tennantite-(Hg) from Binn Valley, Switzerland (Biagioni *et al.*, 2021); tennantite-(Cu) from Arequipa Department, Peru (Biagioni *et al.*, 2022a), tennantite-(Cd) from the Berenguela mining district, Bolivia (Biagioni *et al.*, 2022b)

Chemical data

Quantitative chemical analyses were performed using a Shimadzu1720 electron probe microanalyser at Central South University. Experimental conditions were: wavelength dispersive spectroscopy mode, accelerating voltage = 15 kV, beam current = 10 nA and beam diameter = 1 μm. Standards (element, emission line) were: Cu (Cu*K*α), Ni (Ni*K*α), FeS_2 (Fe*K*α and S*K*α), Sb_2S_3 (Sb*L*α) and FeAsS (As*L*α), and ZAF correction was done. Data for seven electron microprobe analysis are provided in Table 2.

X-ray crystallography and structure refinement

Both powder and single-crystal X-ray studies of tennantite-(Ni) were carried out using a Rigaku XtaLAB Synergy diffractometer (Cu*K*α radiation). The powder X-ray diffraction data were recorded in powder mode at 50 kV and 1 mA. However, though we attempted to collect powder X-ray diffraction data on tennantite-(Ni), our crystal obtained by FIB is only 8 × 6 × 4 μm, and we were only able to measure a few intense reflections (actually only 3). Therefore, we have decided to provide only the *d* spacings from the single-crystal diffraction data. The indexed powder diffraction data for tennantite-(Ni) from single-crystal X-ray diffraction are listed in Table 3.

Single-crystal X-ray studies were performed using a Rigaku XtaLAB Synergy diffractometer equipped with a Hybrid Pixel Array Detector and Cu*K*α radiation at 50 kV and 1 mA from a

Table 2. Chemical data (wt. %) for tennantite-(Ni).*

Element	Mean	Range	S.D. (σ)	Apfu
Cu	43.96	42.48–45.09	0.81	10.53
Ni	3.74	2.79–5.16	0.76	0.97
Fe	1.85	1.67–2.02	0.14	0.50
As	14.47	11.49–15.83	1.41	2.94
Sb	8.49	6.26–12.70	2.20	1.06
S	26.90	26.43–27.57	0.40	12.77
Total	99.42			

*The data are averaged over 7 data points measured over the crystal.

Table 3. X-ray powder diffraction data (*d* in Å) for tennantite-(Ni).*

I_{calc}	d_{calc}	*h k l*	I_{calc}	d_{calc}	*h k l*
10	**3.640**	**2 2 0**	3	1.766	4 3 3
100	**2.972**	**2 2 2**	4	1.670	6 1 1
4	2.752	3 2 1	4	1.628	6 2 0
28	**2.574**	**4 0 0**	**18**	**1.552**	**6 2 2**
5	2.427	3 3 0	3	1.456	7 1 0
3	2.019	4 3 1	**7**	**1.287**	**8 0 0**
3	2.019	5 1 0	5	1.181	6 6 2
10	**1.880**	**5 2 1**	5	1.051	8 4 4
83	**1.820**	**4 4 0**			

*Only reflections with $I > 3$ relative intensities are reported. The seven strongest reflections are given in bold.

https://doi.org/10.1180/mgm.2023.41 Published online by Cambridge University Press

nearly equi-dimensional crystal (~8 × 6 × 4 μm) at the Laboratory of X-ray Crystallography, Central South University, China. The crystal was extracted from the polished thin section by using an FEI Helios NanoLab 600i dual beam system equipped with Focused Ion beam (FIB) and scanning electron microscope (SEM). The intensity data were corrected for X-ray absorption using the multi-scan method and empirical absorption correction was performed using *CrysAlisPro* software spherical harmonics, which was implemented in *SCALE3 ABSPACK* scaling algorithm (Rigaku Oxford Diffraction, 2021). The refined unit-cell parameters are $a = 10.2957(9)$ Å, $V = 1091.4(3)$ Å^3 and space group $I\bar{4}3m$. The crystal structure was determined and refined using *SHELX* (Sheldrick, 2015) and *Olex2* software (Dolomanov *et al.*, 2009). Scattering factors for neutral atoms were used initially: Cu at *M*(2), Cu at *M*(1), As *vs.* Sb at *X*(3) and S at *S*(1) and *S*(2) sites. However, due to the similar scattering factors of Cu ($Z = 29$), Ni ($Z = 28$) and Fe ($Z = 26$), in subsequent refinements the mixed occupancy of the *M*(1) site was appropriately fixed corresponding to the chemical analysis to minimise the *R* factor. Several cycles of isotropic refinement converged to $R_1 = 0.1021$, confirming the correctness of the structural model. The *M*(2) site, which had a rather high U_{eq} value, was split into two position, *M*(2A) and *M*(2B) separated by 1.22(2) Å, in agreement with previous studies (Andreasen *et al.*, 2008; Makovicky *et al.*, 2005; Welch *et al.*, 2018; Biagioni *et al.*, 2021, 2022a, 2022b). Further anisotropic refinement with free site-occupancy factors gave 0.687(12) and 0.157(6) for *M*(2A) and *M*(2B) of the 12*e* and 24*g* positions, respectively. In order to improve the data/parameter ratio, the displacement parameters of *M*(2A) and *M*(2B) were restrained to be the same. The As and Sb site-occupancy factors for the *X*(3) site were fixed corresponding to the chemical analysis. Then the R_1 value dropped significantly to 0.0438. The existence of a Flack factor of 0.57 indicates that the structure is twinned and should be refined as a two-component inversion twin. Finally, the anisotropic structural model for all atoms converged to $R_1 = 0.0423$ for 163 reflections with $F_o > 4\sigma(F_o)$ and 21 refined parameters. The details of the data collection and the final structure refinement are given in Table 4. Atomic coordinates and displacement parameters are given in Table 5, and selected bond distances in Table 6. The bond-valence sums (BVS), calculated using the bond-valence parameters of Brese and O'Keeffe (1991), are shown in Table 7. The crystallographic information file has been deposited with the Principal Editor of *Mineralogical Magazine* and is available as Supplementary material (see below).

Table 4. Information on the structural refinement for tennantite-(Ni).

Crystal data	
Structural formula	$Cu_{10.56}Ni_{0.96}Fe_{0.48}As_{2.94}Sb_{1.06}S_{13}$
Formula weight	1520.25
Crystal size (μm)	8 × 6 × 4
Crystal system	cubic
Space group	$I\bar{4}3m$ (#217)
Unit cell dimensions (Å)	$a = 10.2957(9)$
Volume (Å^3)	1091.4(3)
Z	2
Data collection	
Instrument	Rigaku Synergy
Radiation, wavelength	Cu*Kα*, 1.54184 Å
Temperature (K)	293(2)
F(000)	1409
2θ range (°)	12.158 to 129.59
Total reflections	609
Unique ref. (all)	184
Unique ref. [$F_o > 4\sigma(F_o)$]	163
R_{int}	0.0389
R_σ	0.0193
Range of *h*, *k*, *l*	$-5 \le h \le 8$; $-12 \le k \le 11$; $-10 \le l \le 4$
Refinement	
R [$F_o > 4\sigma(F_o)$]	0.0423
R [all data]	0.0491
wR (on F_o^2) *	0.1158
Goof	1.161
Number of least-squares parameters	21
$\Delta\rho_{max}$, $\Delta\rho_{min}$ (e^- Å^{-3})	1.11 [0.61Å from *X*(3)] −0.69[1.51 Å from *X*(3)]

* $w = 1/[\sigma^2(F_o^2)+(0.0677P)^2+8.3002P]$, where $P=(F_o^2+2F_c^2)/3$

Results and discussion

Raman spectroscopy

In the material studied, Raman bands occur mainly between 150 and 400 cm^{-1} (Fig. 3). The very strong bands assigned to symmetric *X*(3)–*S*(1) stretching (ν_1) and antisymmetric *X*(3)–*S*(1) stretching (ν_3), are found at 381cm^{-1} and 357 cm^{-1}, respectively, which is consistent with the previous Raman spectra study of the tetrahedrite–tennantite solid solutions (Kharbish *et al.*, 2007). According to Apopei *et al.* (2017), tennantite with a ratio of As/(As+Sb) ranging from 1 to 0.56 exhibits a peak shift for ν_1 symmetric stretching from 383 to 378 cm^{-1}. In our case, it has a good agreement with their result, i.e. the chemical composition As/(As+Sb) = 0.735, and ν_1 peaks occurring at 379 cm^{-1}. The ν_2 symmetric bending is a weak band that occurs at 337 cm^{-1}, which is almost overlapped by the two strongest neighbouring stretching modes. The medium band at 312 cm^{-1} is assigned to ν_4 antisymmetric bending, referring to the $X(3)S(1)_3$ group modes. The weak band occurring at 180 cm^{-1} is assigned to lattice vibrations.

Chemical formula

The empirical formula calculated on the basis of 16 cations per formula unit, is $^{M(2)}Cu_6{}^{M(1)}[Cu_{4.00}(Ni_{0.97}Cu_{0.53}Fe_{0.50})_{\Sigma 2}]_{\Sigma 6}{}^{X(3)}(As_{2.94}Sb_{1.06})_{\Sigma 4}S_{12.77}$, which can be simplified as $Cu_6[Cu_4(Ni,Cu,Fe)_2](As,Sb)_4S_{13}$.

In the material studied, the Cu content is close to 10.5 atoms per formula unit (apfu), so the C constituent is represented by Ni, Cu and Fe. Taking into account previous studies, the valence state of iron at the *M*(1) site probably occurs as Fe^{3+} in copper-rich tennantite (Makovicky *et al.*, 2003), in which case the empirical formula of our studied material could be given as $^{M(1)}[^{B}Cu_{4.00}{}^{C}(Ni^{2+}_{0.97}Cu^{2+}_{0.03}Cu^{+}_{0.50}Fe^{3+}_{0.50})]$, on the basis that all the iron is assumed to Fe^{3+}. On the one hand this hypothetical composition can be idealised to the end-member formula $Cu_6[Cu_4(Ni^{2+}Cu^{+}_{0.50}Fe^{3+}_{0.50})]As_4S_{13}$, the site population of Ni^{2+} and $(Cu^{+}_{0.50}Fe^{3+}_{0.50})^{2+}$ are both 1 apfu, following the site-total-charge approach (Bosi *et al.*, 2019), which is exactly the boundary component of tennantite-(Ni) and the potential 'tennantite-(Fe^{3+})' (see the detailed discussion by Biagioni *et al.*, 2022a). On the other hand, in our case, the observed bond distance shows that both copper and iron are mostly divalent in the C constituent, at least not all iron is trivalent (discussed below). In any case, based on the IMA–CNMNC rules for dominant constituents (Hatert and Burke, 2008) and valency-imposed double site-occupancy (Bosi *et al.*, 2019), the material studied is Ni^{2+} dominant in the C constituent. Consequently, the end-member formula of

https://doi.org/10.1180/mgm.2023.41 Published online by Cambridge University Press

Table 5. Atomic coordinates and equivalent isotropic displacement parameters (in Å^2) for tennantite-(Ni).

Site*	*x/a*	*y/b*	*z/c*	U_{eq}	U^{11}	U^{22}	U^{33}	U^{23}	U^{13}	U^{12}
M(2A)	0.7816(9)	0	0	0.041(3)	0.018(3)	0.052(4)	U^{22}	−0.029(4)	0	0
M(2B)	0.791(2)	0.077(2)	−0.077(2)	0.041(3)	0.018(3)	0.052(4)	U^{22}	−0.029(4)	0	0
M(1)	¾	½	0	0.0280(14)	0.030(3)	0.0269(18)	U^{22}	0	0	0
X(3)	0.7385(2)	0.2615(2)	0.2615(2)	0.0216(11)	0.0216(11)	U^{11}	U^{11}	0.0018(10)	$-U^{23}$	$-U^{23}$
S(1)	0.6406(5)	0.1160(4)	0.1160(4)	0.0227(15)	0.016(4)	0.0258(19)	U^{22}	0.002(2)	−0.0023(18)	U^{13}
S(2)	0	0	0	0.027(4)	0.027(4)	U^{11}	U^{11}	0	0	0

*Occupancies: *M*(2A) = $Cu_{0.690(12)}$; *M*(2B) = $Cu_{0.155(6)}$; *M*(1) = $Cu_{0.76}Ni_{0.16}Fe_{0.08}$; *X*(3) = $As_{0.735}Sb_{0.265}$

Table 6. Selected bond distances (Å) for tennantite-(Ni).

M(2A)–S1$^{\times 2}$	2.227(6)	Cu2B–S1$^{\times 2}$	2.55(2)
M(2A)–S2$^{\times 1}$	2.248(9)	Cu2B–S2$^{\times 1}$	2.42(2)
<*M*(2A)–S>	2.234	<Cu(2B)–S>	2.507
Cu2A–Cu2B	1.13(3)	Cu2B–Cu2B	2.23(7)
			1.93(5)
Cu1–S1$^{\times 4}$	2.329(3)	(As,Sb)–S1$^{\times 3}$	2.346(5)

Table 7. Bond-valence sums (vu) for tennantite-(Ni).*

Site	*M*(2)	*M*(1)	*X*(3)	Sum	Theor.
S(1)	0.304$^{\times 2\downarrow}$	0.338$^{\times 4\downarrow \times 2\rightarrow}$	0.934$^{\times 3\downarrow}$	1.913	2.000
S(2)	0.310$^{6\rightarrow}$			1.860	2.000
Sum	0.918	1.352	2.801		
Theor.	1.000	1.333	3.000		

* BVS were calculated with the site-occupancy factors given in Table 5

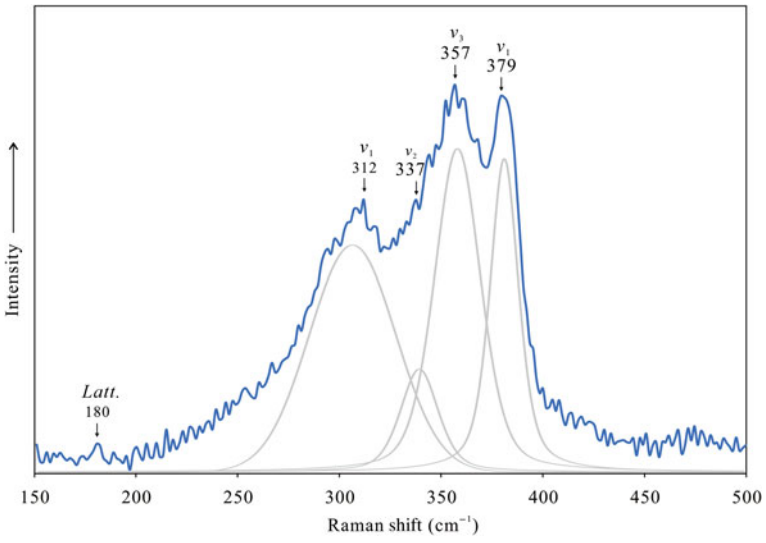

Figure 3. Raman spectrum for tennantite-(Ni).

tennantite-(Ni) is $Cu_6(Cu_4Ni_2)As_4S_{13}$, corresponding to (wt.%) Cu 43.24, Ni 7.99, As 20.40, S 28.37, total 100.

Crystal-structure description

Tennantite-(Ni) is isostructural with other minerals in the tetrahedrite group. Compared to other species belonging to the tetrahedrite group, the *M*(2) site of tennantite and zvěstovite-series minerals (As-dominant at the *X*(3) site) need to be split into two sub-positions, one *M*(2A) and two neighbouring *M*(2B), due to the moderately significant high anisotropic thermal motion at the *M*(2) site (e.g. Wuensch *et al.*, 1966; Makovicky *et al.*, 2005; Sejkora *et al.*, 2021; Biagioni *et al.*, 2021, 2022a, 2022b). Taking into account that an *M*(2) split has also been found in argentotetrahedrite-(Zn) (Sejkora *et al.*, 2022) and rozhdestvenskayaite-(Zn) (Welch *et al.*, 2018), this is likely to be a common feature of tetrahedrite-group minerals.

The structure of tennantites can be described by five non-equivalent crystallographic sites with the general structural formula $^{M(2)}A_6{}^{M(1)}(B_4C_2)^{X(3)}D_4{}^{S(1)}Y_{12}{}^{S(2)}Z$, where *M*(1) cations are tetrahedrally coordinated by four *S*(1), and *X*(3) forms a trigonal pyramid (AsS_3) with three *S*(1). The *S*(2) site is located in the centre of the octahedron (Cu_6S) (Johnson *et al.*, 1988). *M*(2A) is at triangular planar position (CuS_3) coordinated by $S(1)_2S(2)$, while *M*(2B) is at the site above and below the plane of the triangle, exhibiting a flat trigonal pyramid (Fig. 4). In the crystal studied of tennantite-(Ni), the average bond distance of *M*(2A)–*S*(2) and *M*(2B)–*S*(2) are 2.248(9) and 2.42(2) Å, respectively. Such bond-distance values can be compared with the reported split *M*(2) sites occurring in Cu-rich unsubstituted tennantite studied by Makovicky *et al.* (2005), with values of 2.219 Å for *M*(2A) and 2.486 Å for *M*(2B), in addition, tennantite-(Cu) described by Biagioni *et al.* (2022a), reported values of 2.230 for *M*(2A) and 2.307 Å for *M*(2B), respectively. In the truncated tetrahedron, *M*(2A) and *M*(2B) atoms show a larger atomic displacement perpendicular to the plane of the triangle, and separated by a distance of 1.13(3) Å. The neighbouring *M*(2B)–*M*(2B) distance is 2.23(7) Å, which is slightly larger than previously

https://doi.org/10.1180/mgm.2023.41 Published online by Cambridge University Press

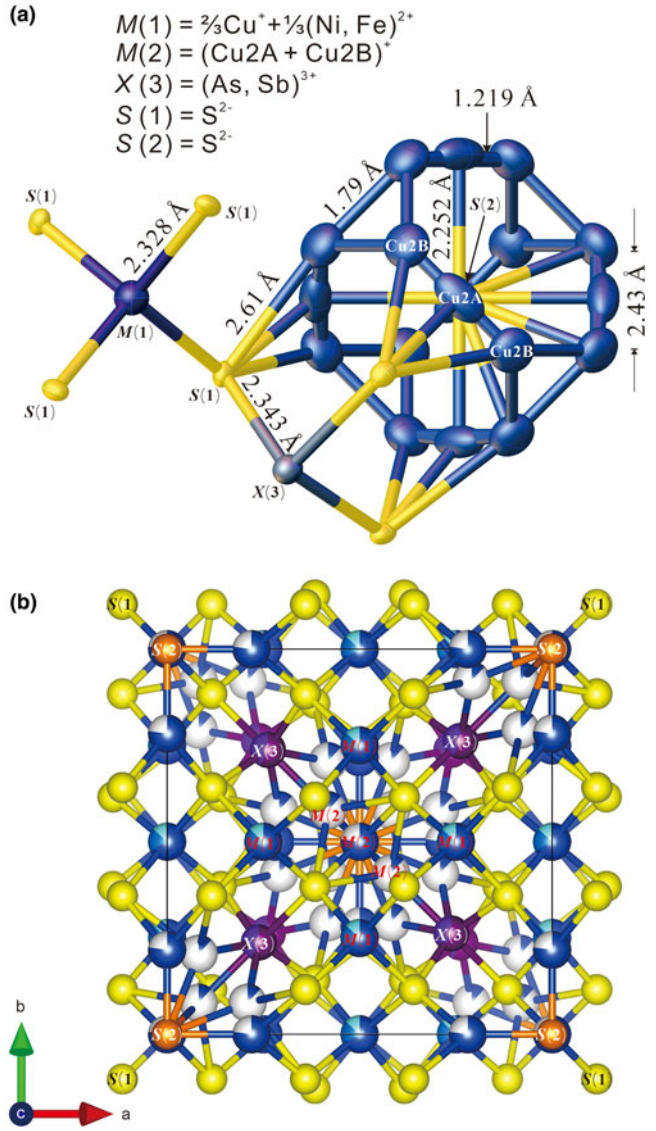

Figure 4. The crystal structure for tennantite-(Ni). (a) Drawn using *Olex2* (Dolomanov, 2009) and (b) drawn using *Vesta* (Momma and Izumi, 2011).

reported tennantite species, e.g. 1.08 Å and 2.15 Å of Cu-rich unsubstituted tennantite (Makovicky *et al.*, 2005); 0.84 Å and 1.68 Å of tennantite-(Cd) (Biagioni *et al.*, 2022b). Clusters of three close *M*(2B) atoms form a regular triangle with edges of 1.93(5) Å. The shortest edge length is to be expected as it is inversely related to the distance of neighbouring *M*(2B). The calculated BVS at the *M*(2) site is 0.918 valence units (vu), in agreement with the full occupancy at this site by monovalent copper.

The tetrahedrally coordinated *M*(1) site is occupied by Cu, Ni and Fe atoms. The resulting occupancy of $Cu_{4.56}Ni_{0.96}Fe_{0.48}$ yields a site-scattering of 173.68 electrons per formula unit (epfu), which is consistent with the calculated value of 171.53 epfu on the basis of chemical data. The average bond distance is 2.329(3) Å, which is shorter than the *M*(1)–*S*(1) distance of tennantite-(Zn) (2.337(8)Å, Wuensch *et al.*, 1966). Following Biagioni *et al.* (2020), the most probable composition of *M*(1) site for the material studied could be $^{M(1)}[^{B}Cu_{4.00}{}^{C}(Ni^{2+}_{0.97}Cu^{2+}_{0.53}Fe^{2+}_{0.50})]$, the calculated distance is 2.292 Å (ionic radii from Shannon, 1976), which is in more agreement with the observed bond distance, than that of the calculated value on the basis of trivalent iron, i.e. $^{M(1)}[^{B}Cu_{4.00}{}^{C}(Ni^{2+}_{0.97}Cu^{2+}_{0.03}Cu^{+}_{0.50}Fe^{3+}_{0.50})]$, corresponding to 2.280 Å. The calculated BVS is 1.352 vu, comparable to the theoretical value of 1.333 vu for ideal occupancy of the *M*(1) site ($⅔Me^{+}+⅓Me^{2+}$).

The *X*(3) site has an average bond distance of 2.346(5) Å, and the value is larger than the average bond distance of other tennantites, e.g. 2.246 Å for tennantite-(Zn) (Wuensch *et al.*, 1966) and 2.266 Å for tennantite-(Cu) (Biagioni *et al.*, 2022a). Taken into account, the ideal As–S and Sb–S distances are 2.26 and 2.46 Å (Johnson *et al.*, 1988), respectively; the difference is attributable to the mixed occupancy of the As/Sb element at this site. The calculated As/Sb atomic ratio on the basis of the observed bond distance, corresponds to 0.57:0.43. If the mixed occupancy of the *X*(3) site was fixed corresponding to the calculated As/Sb atomic ratio, the R_1 will rise from 0.0423 to 0.0438. The slight difference between the chemical component and the ratio calculated on the basis of the observed bond distance is acceptable and indicates that some details in the crystal structure may be affected by the different chemistry of the studied grains. The calculated BVS of 2.801 vu is consistent with the presence of $(As, Sb)^{3+}$.

Genesis of tennantite-(Ni)

The tennantite-(Ni)-hosting listvenites are thought to be the carbonation product of the serpentinisation of mantle peridotites in the Luobusa deposit (Zhang *et al.*, 2015). According to the occurrence and paragenesis, it can be concluded that tennantite-(Ni), gersdorffite, and antigorite–népouite-series minerals were formed in the early stage, and replaced subsequently by the carbonated minerals (e.g. Ni-bearing hydrated arsenate minerals ± magnesite ± quartz ± Cr-rich mica). These mineral assemblages record three stages of nickel migration. Nickel, as a compatible element, has an ionic radius of $^{VI}Ni^{2+}$(0.69 Å) that is similar to $^{VI}Mg^{2+}$(0.72 Å) (Shannon, 1976) and could enter the octahedral site of forsterite in the first stage via partial substitution from the deep Earth. The second stage may occur in the supra-subduction zone (SSZ) environment, where strong serpentinisation results in release of Ni^{2+} cations by the dissolution of forsterite (the major rock-forming minerals of the Luobusa mantle peridotites), and reacts with the Sb/As containing fluid to form tennantite-(Ni), associated chalcogenides and Ni-bearing serpentine-series minerals. The last, listvenitisation stage, is characterised by intense carbonation, replacing early Ni/As-bearing minerals to form hydrous nickel-arsenate minerals. Tennantite-(Ni) is usually found in gersdorffite as small composite inclusions composed of vaesite, chalcostibite, tetrahedrite-(Ni), Ni-rich tetrahedrite-(Fe) and Co-rich tennantite-(Fe). The ore assemblages indicate a complex Cu–Ni–Sb–As–S system, which may form at moderately high-temperature conditions of ~300 to 400°C and 0.1 to 0.3 GPa (Clark and Kullerud, 1963; Barbier *et al.*, 2015; Ferenc *et al.*, 2016).

Conclusions

With the discovery of tennantite-(Ni), tennantite is currently the series with the most divalent transition metals end-members in the tetrahedrite group [i.e. Fe ($Z = 26$), Ni ($Z = 28$), Cu ($Z = 29$), Zn ($Z = 30$), Cd ($Z = 48$) and Hg ($Z = 80$)]. Tennantite-(Ni), the rare natural nickel end-member tetrahedrite-group mineral, gives further information about the chemical variability of tetrahedrite-group minerals. In addition, these ore-mineral

https://doi.org/10.1180/mgm.2023.41 Published online by Cambridge University Press

assemblages from the Luobusa chromitite deposit record the geological process of nickel migration and precipitation.

Acknowledgements. The helpful comments of two anonymous reviewers, Structures Editor Peter Leverett, Associate Editor Koichi Momma, and Principal Editor Stuart Mills are greatly appreciated. This study was supported by the Natural Science Foundation of China (NSFC Grant: 42072054) for XG, National Key R&D Programmes (92062105) for ZY, and YW and KQ acknowledges financial support from China Scholarship Council (CSC) (Grant: 202106400047, 202108575009).

Supplementary material. The supplementary material for this article can be found at https://doi.org/10.1180/mgm.2023.41.

Competing interests. The authors declare none.

References

Andreasen J.W., Makovicky E., Lebech B. and Karup-Møller, S. (2008) The role of iron in tetrahedrite and tennantite determined by Rietveld refinement of neutron powder diffraction data. *Physics and Chemistry of Minerals*, **35**, 447–454.

Apopei A.I., Damian G., Buzgar N., Buzatu A., Andráš P., Milovska S. and Della Ventura G. (2017) The determination of the Sb/As content in natural tetrahedrite–tennantite and bournonite–seligmannite solid solution series by Raman spectroscopy. *Mineralogical Magazine*, **81**, 1439–1456.

Barbier T., Lemoine P., Gascoin S., Lebedev O.I., Kaltzoglou A., Vaqueiro P., Powell A.V., Smith R.I. and Guilmeau E. (2015) Structural stability of the synthetic thermoelectric ternary and nickel-substituted tetrahedrite phases. *Journal of Alloys and Compounds*, **634**, 253–262.

Belov N.V. and Pobedimskaya E.A. (1969) Covelline (klockmannite), chalcocite (acanthite, stromeyerite, bornite), fahlerz. *Soviet Physics Crystallography*, **13**, 843–847.

Biagioni C., George L.L., Cook N.J., Makovicky E., Moëlo Y., Pasero M., Sejkora J., Stanley C.J., Welch M.D. and Bosi F. (2020) The tetrahedrite group: Nomenclature and classification. *American Mineralogist*, **105**, 109–122.

Biagioni C., Sejkora J., Raber T., Roth P., Moëlo Y., Dolníček Z. and Pasero M. (2021) Tennantite-(Hg), $Cu_6(Cu_4Hg_2)As_4S_{13}$, a new tetrahedrite-group mineral from the Lengenbach quarry, Binn, Switzerland. *Mineralogical Magazine*, **85**, 744–751.

Biagioni C., Sejkora J., Moëlo Y., Marcoux E., Mauro D. and Dolníček Z. (2022a) Tennantite-(Cu), $Cu_{12}As_4S_{13}$, from Layo, Arequipa Department, Peru: a new addition to the tetrahedrite-group minerals. *Mineralogical Magazine*, **86**, 331–339.

Biagioni C., Kasatkin A., Sejkora J., Nestola F. and Škoda R. (2022b) Tennantite-(Cd), $Cu_6(Cu_4Cd_2)As_4S_{13}$, from the Berenguela mining district, Bolivia: the first Cd-member of the tetrahedrite group. *Mineralogical Magazine*, **86**, 834–840.

Bosi F., Hatert F., Hålenius U., Pasero M., Miyawaki R. and Mills S.J. (2019) On the application of the IMA-CNMNC dominant-valency rule to complex mineral compositions. *Mineralogical Magazine*, **83**, 627–632.

Brese N.E. and O'Keeffe M. (1991) Bond-valence parameters for solids. *Acta Crystallographica*, **B47**, 192–197.

Clark L.A. and Kullerud G. (1963) The sulfur-rich portion of the Fe-Ni-S system. *Economic Geology*, **58**, 853–885.

Criddle A.J. and Stanley C.J. (1993) *Quantitative Data File for Ore Minerals, 3rd Edition*. Chapman & Hall, London.

Des Cloizeaux M. (1855) Notices Minéralogiques. Sur les formes cristallines de la Dufrénoysite. *Les Annales des Mines*, **5**, 389–398.

Dolomanov O.V., Bourhis L.J., Gildea R.J., Howard J.A.K. and Puschmann H. (2009) OLEX2, A complete structure solution, refinement and analysis program. *Journal of Applied Crystallography*, **42**, 339–341.

Ferenc S., Uher P., Spišiak J. and Šimonová V. (2016) Chromium-and nickel-rich micas and associated minerals in listvenite from the Muránska Zdychava, Slovakia: products of hydrothermal metasomatic transformation of ultrabasic rock. *Journal of Geosciences*, **61**, 239–254.

Hatert F. and Burke E.A. (2008) The IMA–CNMNC dominant-constituent rule revisited and extended. *The Canadian Mineralogist*, **46**, 717–728.

Johnson N.E., Craig J.R. and Rimstidt J.D. (1988) Crystal chemistry of tetrahedrite. *American Mineralogist*, **73**, 389–397.

Kharbish S., Libowitzky E. and Beran, A. (2007) The effect of As-Sb substitution in the Raman spectra of tetrahedrite-tennantite and pyrargyrite-proustite solid solutions. *European Journal of Mineralogy*, **19**, 567–574.

Makovicky E., Tippelt G., Forcher K., Lottermoser W., Karup-Møller S. and Amthauer, G. (2003). Mössbauer study of Fe-bearing synthetic tennantite. *The Canadian Mineralogist*, **41**, 1125–1134.

Makovicky E., Karanović L., Poleti D., Balić-Žunić T. and Paar W.H. (2005) Crystal structure of copper-rich unsubstituted tennantite, $Cu_{12.5}As_4S_{13}$. *The Canadian Mineralogist*, **43**, 679–688.

Moëlo Y., Makovicky E., Mozgova N.N., Jambor J.L., Cook N., Pring A., Paar W., Nickel E.H., Graeser S., Karup-Møller S., Bali- Žunić T., Mumme W.G., Vurro F., Topa D., Bindi L., Bente K. and Shimizu M. (2008) Sulfosalt systematics: a review. Report of the sulfosalt sub-committee of the IMA Commission on Ore Mineralogy. *European Journal of Mineralogy*, **20**, 7–46.

Momma K. and Izumi F. (2011) VESTA 3 for three-dimensional visualization of crystal, volumetric and morphology data. *Journal of Applied Crystallography*, **44**, 1272–1276.

Nakamoto K. (1997) *Infrared and Raman spectra of inorganic and coordination compounds. Part A: Theory and applications in inorganic chemistry*. 5th ed., Wiley-Interscience New York, 408 pp.

Nyman H. and Hyde B.G. (1981) The related structures of α-Mn, sodalite, Sb_2Tl_7, etc. *Acta Crystallographica*, **A37**, 11–17.

Pauling L. and Neuman E.W. (1934) The crystal structure of binnite (Cu, Fe)$_{12}As_4S_{13}$ and the chemical composition and structure of minerals of the tetrahedrite group. *Zeitschrift für Kristallographie*, **88**, 54–62.

Phillips R. (1819) Analysis of the copper ore, described in the preceding paper. *The Quarterly Journal of Science, Literature and the Arts*, **7**, 100–102.

Phillips W. (1819) Description of an ore of copper from Cornwall. *The Quarterly Journal of Science, Literature and the Arts*, **7**, 95–100.

Rigaku Oxford Diffraction (2021) *CrysAlisPro Software system, version 1.171.41.96a*. Rigaku Corporation.

Sack R.O. and Ebel D.S. (1993) As–Sb exchange energies in tetrahedrite-tennantite fahlores and bournonite-seligmannite solid solutions. *Mineralogical Magazine*, **57**, 635–642.

Sejkora J., Biagioni C., Vrtiška L. and Moëlo Y. (2021) Zvěstovite-(Zn), $Ag_6(Ag_4Zn_2)As_4S_{13}$, a new tetrahedrite-group mineral from Zvěstov, Czech Republic. *Mineralogical Magazine*, **85**, 716–724.

Sejkora J., Biagioni C., Števko M., Raber T., Roth P. and Vrtiška, L. (2022) Argentotetrahedrite-(Zn), $Ag_6(Cu_4Zn_2)Sb_4S_{13}$, a new member of the tetrahedrite group. *Mineralogical Magazine*, **86**, 319–330.

Shannon R.D. (1976) Revised effective ionic radii and systematic studies of interatomic distances in halides and chalcogenides. *Acta Crystallographica*, **A32**, 751–767.

Sheldrick G.M. (2015) SHELXT–Integrated space-group and crystal structure determination. *Acta Crystallographica*, **A71**, 3–8.

Wang Y, Chen R, Gu X, Yang Z, Hou Z, Fan G, Ye L and Qu K (2021) Tennantite-(Ni), IMA 2021-018. CNMNC Newsletter 62. *Mineralogical Magazine*, **62**, 634–638, https://doi.org/10.1180/mgm.2021.62.

Warr L.N. (2021) IMA–CNMNC approved mineral symbols. *Mineralogical Magazine*, **85**, 291–320.

Welch M.D., Stanley C.J., Spratt J. and Mills S.J. (2018) Rozhdestvenskayaite $Ag_{10}Zn_2Sb_4S_{13}$ and argentotetrahedrite $Ag_6Cu_4(Fe^{2+},Zn)_2Sb_4S_{13}$: two Ag-dominant members of the tetrahedrite group. *European Journal of Mineralogy*, **30**, 1163–1172.

Wuensch B.J., Takéuchi Y. and Nowacki W. (1966) Refinement of the crystal structure of binnite, $Cu_{12}As_4S_{13}$. *Zeitschrift für Kristallographie*, **123**, 1–20.

Xiong F.H., Yang J.S., Robinson P. T., Xu, X.Z., Liu Z., Li Y., Li J.Y and Chen S.Y. (2015) Origin of podiform chromitite, a new model based on the Luobusa ophiolite, Tibet. *Gondwana Research*, **27**, 525–542.

Yang J.S., Bai W.J., Fang Q.S., Yan B.G., Rong H. and Chen S.Y. (2004) Coesite discovered from the podiform chromitite in the Luobusa ophiolite, Tibet. *Earth Science: Journal of China University of Geosciences*, **29**, 651–660 [in Chinese with English abstract].

Zhang L., Yang J.S., Robinson P.T., Xiong F.H., Chen Y.H., Lai S.M. and Chen M. (2015) Origin of listwanite in the Luobusa ophiolite, Tibet, implications for chromite stability in hydrothermal systems. *Acta Geologica Sinica – English Edition*, **89**, 402–417.

Zhou M.F., Robinson P.T., Malpas J. and Li Z. (1996) Podiform chromitites from the Luobusa ophiolite (southern Tibet): implications for melt–rock interaction and chromite segregation. *Journal of Petrology*, **37**, 3–21.

https://doi.org/10.1180/mgm.2023.41 Published online by Cambridge University Press